Exp Fluids (2008) 44:831–842
DOI 10.1007/s00348-007-0439-3

RESEARCH ARTICLE

On velocity gradients in PIV interrogation

J. Westerweel

Received: 20 April 2007 / Revised: 11 November 2007 / Accepted: 28 November 2007 / Published online: 29 December 2007

Abstract This paper presents a generalization of the description of the displacement-correlation peak in particle image velocimetry (PIV) to include the effects due to local velocity gradients at the scale of the interrogation domain. A general expression is derived that describes the amplitude, location and width of the displacement-correlation peak in the presence of local velocity gradients. Simplified expressions are obtained for the peak centroid and peak width for simple non-uniform motions. The results confirm that local gradients can be ignored provided that the variation of the displacement within the interrogation domain does not exceed the (mean) particle-image diameter. An additional bias occurs for a spatially accelerating or decelerating fluid, which implies an artificial "particle inertia" even when the particles can be considered as ideal tracers.

1 Introduction

In the interrogation analysis in particle image velocimetry (PIV) by means of a spatial correlation, it is generally assumed that the displacement field is uniform (Adrian 1988; Westerweel 1993, 1997; Olsen and Adrian 2001). However, PIV is applied to study the flow fields that are typically non-uniform, and therefore it has to be explained under what circumstances the displacement field can be considered to be uniform at the scale of the interrogation volume. In the preceding studies for the case of uniform displacement fields it was shown that the width of the displacement-correlation peak is proportional to the particle-image diameter d_τ (Adrian 1988; Westerweel 2000b). In a simulation study it was shown that the velocity gradients can be ignored when the variation a of the local particle-image displacement is small with respect to d_τ (Keane and Adrian 1992), i.e.,

$$|a| \ll d_\tau \quad \text{with} \quad a \equiv M\Delta u\Delta t, \tag{1}$$

where M is the image magnification, Δt is the exposure time delay, and Δu represents the local variation of the velocity field, i.e.,

$$|\Delta u| \sim |\partial \boldsymbol{u}/\partial \boldsymbol{x}| \cdot L, \tag{2}$$

where L is a typical dimension of the interrogation volume, e.g., the thickness of the light sheet Δz_0 or the equivalent in-plane dimension of the interrogation region D_I/M. The effect on the appearance of the correlation as a function of an increasing variation a of the displacement within the interrogation volume is shown in Fig. 1. In many practical situations the ratio d_τ/D_I is very small, and typically should not exceed 3–5% in order to preserve a well-defined correlation peak (Keane and Adrian 1992). This means that the local gradients have to be small in order to comply with this requirement. For increasing gradients the correlation peak amplitude decreases, while the width of the correlation peak increases in proportion to the variation of the displacement. Such a broadening of the displacement-correlation peak also occurs in micro-PIV as the result of Brownian motion of the tracer particles (Olsen and Adrian 2000a), which can be used to estimate the local temperature-dependent viscosity (Hohreiter et al. 2002).

For uniform displacements the correlation peak detectability is proportional to $N_\mathrm{I}\, F_\mathrm{I}\, F_\mathrm{O}$, where N_I is the image

J. Westerweel (✉)
Laboratory for Aero and Hydrodynamics,
Delft University of Technology, Mekelweg 2,
2628 CD Delft, The Netherlands
e-mail: j.westerweel@tudelft.nl

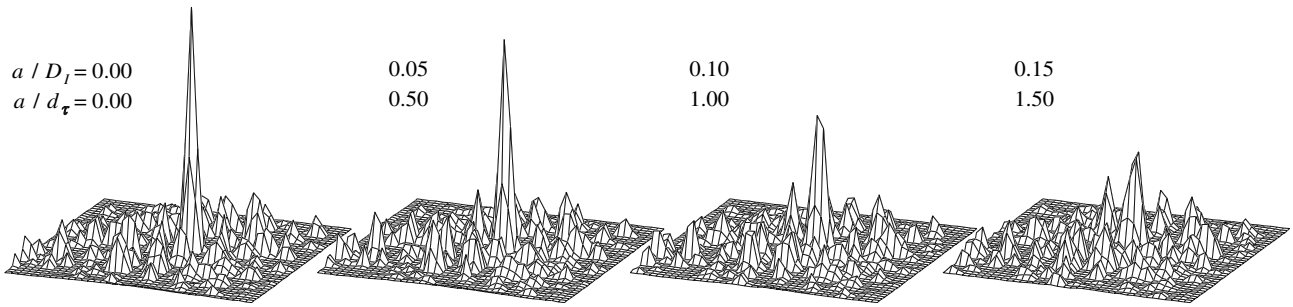

Fig. 1 The spatial correlation for an increasing displacement variation a, defined in Eq. (1), relative to the dimension of the interrogation domain D_I and particle-image diameter d_τ. The approximate peak amplitudes are 1.00, 0.86, 0.55 and 0.40. Adapted from Westerweel (2004)

density and F_I and F_O are the in-plane and out-of-plane loss-of-correlation due to in-plane and out-of-plane motion of the tracer particles (Keane and Adrian 1990). This can be generalized to: $N_\mathrm{I}\, F_\mathrm{I}\, F_\mathrm{O} F_\Delta$, where the term F_Δ accounts for the loss-of-correlation due to the local variation of the displacement field (Westerweel 2004; Hain and Kähler 2007).

The reduction of the displacement-correlation peak means that the peak detectability is reduced. This implies a higher occurrence of spurious vectors in regions with strong local gradients (Keane and Adrian 1992). If the gradient *only* occurs in the in-plane components of the displacement, then it is possible to (partially) compensate for the effects of the gradients in the displacement by means of local image deformation (Huang et al. 1993; Tokumaru and Dimotakis 1995; Fincham and Delerce 2000; Scarano 2002). However, in most turbulent flows the small-scale turbulence is (nearly) isotropic, which means that the in-plane variation of the displacements are of the same magnitude as the out-of-plane variation of the displacements when the light-sheet thickness is of the order of the in-plane dimension of the interrogation domain; then the out-of-plane gradients cannot be compensated by planar deformation methods, which means that the local velocity gradients irreversibly deteriorate the interrogation performance. In multi-frame PIV local velocity gradients can easily dominate the peak detectability when the temporal separation of the interrogation images is increased (Hain and Kähler 2007). For micro-PIV the depth-of-correlation (Olsen and Adrian 2000b) can be of the order of the flow domain (i.e., channel depth), which means that a large range of displacements can occur in a single interrogation domain. As mentioned before, Brownian motion of the tracer particles adds to the broadening of the correlation peak.

In this paper, the mathematical support for the empirical relation in Eq. (1) is derived. First the theoretical analysis for PIV interrogation in case of a uniform displacement field is summarized (Sect. 2). Then an expression for the local displacement distribution is derived (Sect. 3). This is used to generalize the existing theory for uniform displacements to include non-uniform displacement fields (Sect. 4). The analysis follows a more rigorous approach than used by Olsen and Adrian (2001). Based on the extended description several effects are described where local gradients affect the interrogation analysis. The last section (Sect. 5) summarizes the main results.

2 Interrogation by spatial cross-correlation

The point of departure for the analysis is the original theoretical description of the interrogation analysis given by Adrian (1988), Keane and Adrian (1990), Westerweel (1993), and Olsen and Adrian (2001), which is summarized here.

Consider two image fields I_1 and I_2, which represent the two image frames recorded with a time delay $\Delta t = t_2 - t_1$ (Olsen and Adrian 2001):

$$I_1(\boldsymbol{X}) = W_1(\boldsymbol{X}-\boldsymbol{X}_1)\int I_{01}(\boldsymbol{x})\tau_0(\boldsymbol{X}-M\boldsymbol{x})g(\boldsymbol{x},t_1)\mathrm{d}\boldsymbol{x},$$
$$I_2(\boldsymbol{X}) = W_2(\boldsymbol{X}-\boldsymbol{X}_2)\int I_{02}(\boldsymbol{x}')\tau_0(\boldsymbol{X}-M\boldsymbol{x}')g(\boldsymbol{x}',t_2)\mathrm{d}\boldsymbol{x}' \tag{3}$$

where W_1 and W_2 are the weighting functions that define the interrogation windows, I_{01} and I_{02} define the illumination pulses, τ_0 is the particle-image intensity per unit illumination, M the image magnification,[1] $\boldsymbol{X}$ and $\boldsymbol{x}$ are the coordinates in the image domain and flow field domain, respectively, and

$$g(\boldsymbol{x},t) = \sum_i \delta[\boldsymbol{x}-\boldsymbol{x}_i(t)] \tag{4}$$

describes the pattern of tracer particles at positions $\boldsymbol{x}_i(t)$ at time t. It is common to split g into mean and fluctuating

[1] Note that M is only a scalar in the case of paraxial imaging and a thin light sheet; in general M will be a projection matrix that maps $\boldsymbol{x}$ onto $\boldsymbol{X}$; see, e.g., Prasad (2000).

parts, i.e., $g = \langle g \rangle + g'$, with $\langle g \rangle = C$ and $\langle g' \rangle = 0$, where C is the mean number density of tracer particles (Adrian 1988).

The spatial cross-correlation $R(\boldsymbol{s})$ for *continuous* image fields is defined by

$$R(\boldsymbol{s}) = \int I_1(\boldsymbol{X}) I_2(\boldsymbol{X}+\boldsymbol{s}) \mathrm{d}\boldsymbol{X}. \tag{5}$$

For discrete image fields, i.e., digital PIV images, the spatial correlation is also defined at discrete separations. This is given by convoluting $R(\boldsymbol{s})$ with the self-correlation of the spatial pixel sensitivity and sampling the result at discrete separations, as described by Westerweel (1993, 1997). For sufficiently large particle images, i.e., $d_\tau/d_r \ll 1$ (where d_r is the pixel size), $R(\boldsymbol{s})$ closely approximates the spatial correlation for digital PIV images (Westerweel 2000a, b).

It is common to split the image fields into mean and fluctuating parts. Then $R(\boldsymbol{s})$ can be written as (Keane and Adrian 1992)

$$R(\boldsymbol{s}) = R_C(\boldsymbol{s}) + R_F(\boldsymbol{s}) + R_D(\boldsymbol{s}), \tag{6}$$

where R_C is the correlation of the mean image intensities, R_F the correlation of the mean image intensity of I_1 with the fluctuating part of I_2 and vice versa,[2] and R_D the correlation of the fluctuating parts of I_1 and I_2. The terms R_C and R_F vanish when the mean image intensity is subtracted from I_1 and I_2. The remaining term R_D can be split into mean and fluctuating parts, where the averaging is taken over an ensemble of tracer patterns for a given (fixed) velocity field $\boldsymbol{u}(\boldsymbol{X},t)$ (Adrian 1988; Westerweel 1993):

$$R(\boldsymbol{s}) = \langle R_D(\boldsymbol{s}) | \boldsymbol{u} \rangle + R'_D(\boldsymbol{s}) \tag{7}$$

where $\langle R_D(\boldsymbol{s})|\boldsymbol{u}\rangle$ is commonly referred to as the *displacement-correlation peak* and $R'_D(\boldsymbol{s})$ as the *random correlation term* (Westerweel 2000b).

At this point it is common to make a number of general assumptions: (1) that all particle images have an identical shape and size;[3] (2) that the light sheet intensity distribution is only a function of the out-of-plane coordinate[4] (here denoted as z); (3) that the optical axis is normal to the light-sheet plane; and (4) that the two exposures of the light sheet occur in the same plane. The ensemble mean of the spatial correlation can then be written as (Adrian 1988; Westerweel 1993):

$$\begin{aligned}\langle R_D(\boldsymbol{s})|\boldsymbol{u}\rangle = & \frac{1}{M^4}\int W_1(\boldsymbol{X}) W_2(\boldsymbol{X}+\boldsymbol{s}) \\ & \times \iint \tau_0(\boldsymbol{X}-\boldsymbol{X}')\tau_0(\boldsymbol{X}+\boldsymbol{s}-\boldsymbol{X}'') \iint I_{01}(z') I_{02}(z'') \\ & \times \left\langle g'_1\left(\frac{X'}{M},\frac{Y'}{M},z'\right) g'_2\left(\frac{X''}{M},\frac{Y''}{M},z''\right) \middle| \boldsymbol{u} \right\rangle \\ & \times \mathrm{d}z'\mathrm{d}z''\mathrm{d}\boldsymbol{X}\mathrm{d}\boldsymbol{X}'\mathrm{d}\boldsymbol{X}''\end{aligned} \tag{8}$$

where $\langle g'_1(\boldsymbol{x}') g'_2(\boldsymbol{x}'') | \boldsymbol{u} \rangle$ is the conditional two-point ensemble cross-correlation over all possible tracer pattern fluctuations for a given flow field $\boldsymbol{u}$. For a *uniform* displacement this can be expressed as (Adrian 1988)

$$\left\langle g'_1(\boldsymbol{x}') g'_2(\boldsymbol{x}'') | \boldsymbol{u} \right\rangle = C\delta[\boldsymbol{x}'' - \boldsymbol{x}' - \Delta\boldsymbol{x}] \tag{9}$$

with: $\Delta\boldsymbol{x} = \boldsymbol{u}\Delta t$. Under the condition that the particle-image diameter is small with respect to the typical dimension of the interrogation region ($d_\tau \ll D_I$) and for a uniform particle-image displacement $\boldsymbol{s}_D$ ($=M\Delta\boldsymbol{x}$),[5] the displacement-correlation peak can be expressed as (Adrian 1988)

$$\langle R_D(\boldsymbol{s})|\boldsymbol{u}\rangle = I_{z1} I_{z2} N_\mathrm{I} F_\mathrm{I}(\boldsymbol{s}) F_\mathrm{O}(\Delta z) \tau_{00}^2 F_\tau(\boldsymbol{s} - \boldsymbol{s}_D) \tag{10}$$

with:

$$N_\mathrm{I} = C\Delta z_0 D_\mathrm{I}^2 / M^2, \tag{11}$$

$$F_\mathrm{I}(\boldsymbol{s}) = \int W_1(\boldsymbol{X}) W_2(\boldsymbol{X}+\boldsymbol{s}) \mathrm{d}\boldsymbol{X} \Big/ D_\mathrm{I}^2, \tag{12}$$

$$F_\mathrm{O}(\Delta z) = \int I_{01}(z) I_{02}(z+\Delta z)\mathrm{d}z \Big/ \int I_{01}(z) I_{02}(z)\mathrm{d}z, \tag{13}$$

$$F_\tau(\boldsymbol{s}) = \int \tau_0(\boldsymbol{X})\tau_0(\boldsymbol{X}+\boldsymbol{s}) / \tau_{00}^2 \tag{14}$$

with $\tau_{00}^2 = \int \tau_0(\boldsymbol{X})^2 \, \mathrm{d}\boldsymbol{X}$ and $I_{zk} = \int I_{0k}(z) \, \mathrm{d}z$ for $k = 1,2$. The *image density* N_I represents the mean number of particle images in the interrogation domain, the terms F_I and F_O are denoted as the *in-plane* and *out-of-plane loss of correlation*, respectively, and F_τ represents the particle-image self-correlation. Under the assumptions stated above, the displacement-correlation peak is a single sharp peak located at $\boldsymbol{s}_D$. The exact position of the peak can be determined from either the peak centroid or peak maximum. For symmetric particle images and a uniform displacement the peak centroid and peak maximum are identical in the limit $d_\tau/D_\mathrm{I} \to 0$.

The centroid $\boldsymbol{\mu}_D$ of the ensemble mean of the displacement-correlation peak is defined as (Adrian 1988; Keane and Adrian 1990)

$$\boldsymbol{\mu}_D \equiv \frac{\int \boldsymbol{s}\langle R_D(\boldsymbol{s})|\boldsymbol{u}\rangle \mathrm{d}\boldsymbol{s}}{\int \langle R_D(\boldsymbol{s})|\boldsymbol{u}\rangle \mathrm{d}\boldsymbol{s}}. \tag{15}$$

Substitution of Eq. (10) in Eq. (15) yields

[2] In older texts the term R_F is mistakenly referred to as the random correlation term, but this part of the signal is actually included in R_D; (see Westerweel 2000b).

[3] This assumption is generally satisfied for diffraction-limited imaging of small tracer particles; see Adrian (1984). These particle images can have different intensities based on their position within the light sheet.

[4] This condition is generally satisfied at the local scale of the equivalent interrogation volume in the flow.

[5] Note that M is a projection of the volumetric flow domain onto the planar image domain.

$$\boldsymbol{\mu}_D = \frac{\int \boldsymbol{s} F_{\mathrm{I}}(\boldsymbol{s}) F_\tau(\boldsymbol{s} - \boldsymbol{s}_D)\mathrm{d}\boldsymbol{s}}{\int F_{\mathrm{I}}(\boldsymbol{s}) F_\tau(\boldsymbol{s} - \boldsymbol{s}_D)\mathrm{d}\boldsymbol{s}}. \tag{16}$$

The function $F_\tau(\boldsymbol{s})$ is symmetric with its centroid located at $\boldsymbol{s}_D$. The in-plane loss-of-correlation $F_{\mathrm{I}}(\boldsymbol{s})$ *skews* $F_\tau(\boldsymbol{s} - \boldsymbol{s}_D)$, which leads to a bias error in the measured displacement (Keane and Adrian 1990; Westerweel 1997). The bias error is directed toward smaller displacements, which is related to the fact that particle images with larger displacements are more likely to leave the interrogation domain between the two light pulses.

In general the width of $F_\tau(\boldsymbol{s})$ is much smaller than the width of $F_{\mathrm{I}}(\boldsymbol{s})$, i.e., $d_\tau \ll D_{\mathrm{I}}$. Hence, $F_{\mathrm{I}}(\boldsymbol{s})$ can be written as a Taylor series around $\boldsymbol{s}_D$:

$$F_{\mathrm{I}}(\boldsymbol{s}) = F_{\mathrm{I}}(\boldsymbol{s}_D) + (\boldsymbol{s} - \boldsymbol{s}_D) \cdot \left.\frac{\partial F_{\mathrm{I}}}{\partial \boldsymbol{s}}\right|_{\boldsymbol{s}=\boldsymbol{s}_D} + \text{h.o.} \tag{17}$$

Substitution in Eq. (16) yields

$$\boldsymbol{\mu}_D \cong \boldsymbol{s}_D + \frac{1}{F_{\mathrm{I}}(\boldsymbol{s}_D)} \cdot \left[\frac{\int s^2 F_\tau(\boldsymbol{s})\mathrm{d}\boldsymbol{s}}{\int F_\tau(\boldsymbol{s})\mathrm{d}\boldsymbol{s}}\right] \cdot \left.\frac{\partial F_{\mathrm{I}}}{\partial \boldsymbol{s}}\right|_{\boldsymbol{s}=\boldsymbol{s}_D} \tag{18}$$

where the term between brackets is the second moment of $F_\tau(\boldsymbol{s})$. Given that $F_{\mathrm{I}}(\boldsymbol{s})$ and the second moment of $F_\tau(\boldsymbol{s})$ are both positive, and that $\partial F_{\mathrm{I}}/\partial \boldsymbol{s}$ is directed toward the origin, $\boldsymbol{\mu}_D$ is usually biased toward $\boldsymbol{s} = \boldsymbol{0}$ (Keane and Adrian 1990; Westerweel 1997).

For identical square uniform interrogation windows, the in-plane loss-of-correlation is given by Westerweel (1997):

$$F_{\mathrm{I}}(s,t) = \begin{cases} (1 - |s|/D_{\mathrm{I}})(1 - |t|/D_{\mathrm{I}}) & \text{for } |s|, |t| < D_{\mathrm{I}}, \\ 0 & \text{elsewhere.} \end{cases} \tag{19}$$

To reduce the complexity of the analysis, only one component of $\boldsymbol{s}$ is considered. The spatial derivative of F_{I} with respect to s is then given by

$$\left.\frac{\partial F_{\mathrm{I}}}{\partial s}\right|_{s=s_D} = -\frac{1}{D_{\mathrm{I}}} \frac{s_D}{|s_D|} \frac{1}{1 - |t_D|/D_{\mathrm{I}}} \tag{20}$$

with $\boldsymbol{s}_D = (s_D, t_D)$. (A similar expression can be found for the direction perpendicular to the direction of s). The second moment of $F_\tau(\boldsymbol{s})$ for identical Gaussian particle images is $\frac{1}{8} d_\tau^2$, so that the expression for the expected correlation peak centroid defined in Eq. (18) becomes:

$$\mu_D = s_D - \frac{s_D}{|s_D|} \frac{1}{1 - |s_D|/D_{\mathrm{I}}} \frac{d_\tau^2}{8 D_{\mathrm{I}}}. \tag{21}$$

As the second order and higher order derivatives for F_{I} defined in Eq. (19) in are zero, this expression is exact. Indeed, the centroid is biased toward $s = 0$. For uniform interrogation regions the displacement bias error is practically constant over a considerable range in $\boldsymbol{s}_D$ (Westerweel 1997).

In general the bias error will be small, i.e., typically about 0.06 px for particle images with a diameter of 2 px in a 32 × 32-pixel interrogation domain (Westerweel 1997). This is small with respect to the random error (typically 0.1 pixel units) in instantaneous data, but can be significant when evaluating flow statistics, such as the mean flow velocity. The bias error can be eliminated in several ways. It is evident that the bias error vanishes when the gradient of F_{I} is zero. For uniform interrogation windows this can be accomplished either by using two interrogation windows of different size (Keane and Adrian 1992), or by using offset interrogation regions (Westerweel et al. 1997), so that the displacement-correlation peak is located at the *maximum* of $F_{\mathrm{I}}(\boldsymbol{s})$ (i.e., $\partial F_{\mathrm{I}}/\partial \boldsymbol{s} = 0$). Another approach is to divide the correlation values by $F_{\mathrm{I}}(\boldsymbol{s})$ (Westerweel 1997).

3 The distribution function of a displacement field

In this section it is explained how the displacement distribution is obtained for a given displacement field over a finite measurement volume. The evaluation of the images by a spatial cross-correlation implies that $\langle g'_1 g'_2 | \boldsymbol{u} \rangle$ is evaluated over a finite measurement volume, i.e., $\delta V(\boldsymbol{x}') = \Delta z_0 \cdot (D_{\mathrm{I}}/M)^2$, which is depicted in Fig. 2. This volume is equivalent to the weight function $W(\boldsymbol{x})$ defined by Olsen and Adrian (2001). Due to the spatial variations in the displacement over $\delta V(\boldsymbol{x}')$, the single displacement value that is represented by the δ-function in Eq. (9) is replaced by a displacement *distribution* function $F_\Delta(\boldsymbol{s})$, which eliminates the explicit dependence on $\boldsymbol{x}'$ and leads to the following expression for the displacement-correlation peak:

$$\langle R_D(\boldsymbol{s}) | \boldsymbol{u} \rangle \cong I_z^2 \tau_{00}^2 \cdot N_{\mathrm{I}} F_{\mathrm{I}} F_{\mathrm{O}} \cdot F_\tau * F_\Delta(\boldsymbol{s}) \tag{22}$$

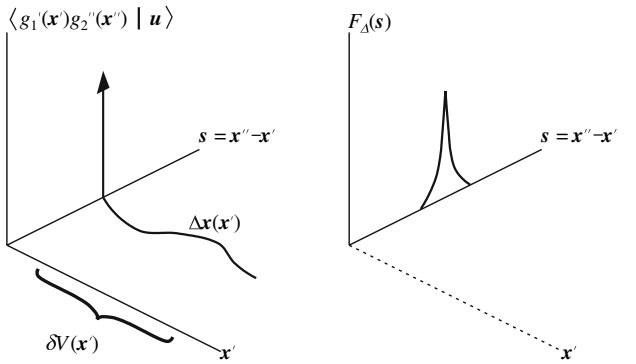

Fig. 2 The integration of $\langle g'_1 g'_2 | \boldsymbol{u} \rangle$ over a small volume $\delta V(\boldsymbol{x}')$ is replaced by a displacement distribution $F_\Delta(\boldsymbol{s})$. (The axes for $\boldsymbol{x}'$ and $\boldsymbol{x}'' - \boldsymbol{x}'$ actually represent three-dimensional spaces.) Adapted from Westerweel (1997)

where * represents a convolution integral. Hence, the displacement $\boldsymbol{s}_D$ is no longer uniquely defined: it may now refer to the maximum of $F_\Delta(\boldsymbol{s})$ (viz., the most probable displacement), or the first moment of the distribution (viz., the local mean displacement), or any other convenient parameter that characterizes $F_\Delta(\boldsymbol{s})$.

The displacement distribution for a displacement field $\Delta\boldsymbol{x}(\boldsymbol{x})$ over a finite measurement volume δV is given by

$$F_\Delta(\boldsymbol{s}) = \frac{1}{\delta V}\int_{\delta V} \delta[\boldsymbol{s} - \Delta\boldsymbol{x}(\boldsymbol{x})]\mathrm{d}\boldsymbol{x}. \tag{23}$$

This integral can be easily evaluated in the Fourier transform domain, i.e.

$$\begin{aligned}\mathcal{F}\{F_\Delta(\boldsymbol{s})\} &= \int \frac{1}{\delta V}\int_{\delta V} \delta[\boldsymbol{s} - \Delta\boldsymbol{x}(\boldsymbol{x})]\mathrm{e}^{2\pi\mathrm{i}\boldsymbol{k}\cdot\boldsymbol{s}}\,\mathrm{d}\boldsymbol{x}\mathrm{d}\boldsymbol{s} \\ &= \frac{1}{\delta V}\int_{\delta V} \mathrm{e}^{2\pi\mathrm{i}\boldsymbol{k}\cdot\Delta\boldsymbol{x}(\boldsymbol{x})}\,\mathrm{d}\boldsymbol{x}\end{aligned} \tag{24}$$

where the following identity was applied:

$$\int \delta(\boldsymbol{x} - \boldsymbol{x}_0)\mathrm{e}^{2\pi\mathrm{i}\boldsymbol{k}\cdot\boldsymbol{x}}\mathrm{d}\boldsymbol{x} = \mathrm{e}^{2\pi\mathrm{i}\boldsymbol{k}\cdot\boldsymbol{x}_0}. \tag{25}$$

Note that: $\mathcal{F}\{F_\Delta(\boldsymbol{s})\} \equiv 1$, for $\boldsymbol{k} = \boldsymbol{0}$, i.e.: $\int F_\Delta(\boldsymbol{s})\mathrm{d}\boldsymbol{s} \equiv 1$, so that $F_\Delta(\boldsymbol{s})$ is indeed a distribution function for arbitrary $\Delta\boldsymbol{x}(\boldsymbol{x})$.

To illustrate the effect of a local variation of the displacement field, two example displacement fields are considered: a simple shear and a sinusoidal displacement field. First, consider a simple shear in one direction, i.e.,

$$\Delta\boldsymbol{x}(\boldsymbol{x}) = (ay, 0, 0)^T \tag{26}$$

for $-L \le y \le L$, where a is a constant. Consider only the x-coordinate, which implies a reduction to a one-dimensional problem. Substitution of Eq. (26) in Eq. (24) yields

$$\begin{aligned}\mathcal{F}\{F_\Delta(s)\} &= \int_{-\infty}^{\infty} \frac{1}{2L}\int_{-L}^{L} \delta(s - ax)\mathrm{e}^{2\pi\mathrm{i}ks}\mathrm{d}x\,\mathrm{d}s \\ &= \frac{1}{2L}\int_{-L}^{L} \mathrm{e}^{2\pi\mathrm{i}kax}\mathrm{d}x = \mathrm{sinc}(2kaL).\end{aligned} \tag{27}$$

The inverse Fourier transform of a sinc-function is a rect-function

$$\mathrm{sinc}(bk) \xrightarrow{\mathcal{F}^{-1}} \frac{1}{b}\mathrm{rect}(s/b) = \begin{cases} 1/b & \text{for } |s| < b/2, \\ 0 & \text{elsewhere,}\end{cases} \tag{28}$$

so that the inverse Fourier transform of Eq. (27) yields

$$F_\Delta(s) = \frac{1}{2aL}\mathrm{rect}\left(\frac{s}{2aL}\right). \tag{29}$$

Note that the total area of the rect-function is unity. This implies that an increase of the shear also increases the width of the distribution, but decreases the amplitude. Hence, the local variations of the displacement *reduce* the correlation peak amplitude and *increase* the width of the correlation peak, in correspondence to what occurs in Fig. 1 for increasing a. Consequently, the local variations of the displacement field also *reduce* the peak detectability, and *enhance* the displacement bias error.

Now, consider a sinusoidal displacement field, again in one direction only, i.e.,

$$\Delta\boldsymbol{x}(\boldsymbol{x}) = (\sin(\pi y/L), 0, 0)^T \tag{30}$$

over the domain $-L \le x \le L$. The corresponding Fourier transform of the displacement distribution is equal to a zeroth order Bessel function of the first kind, i.e.,

$$\begin{aligned}\mathcal{F}\{F(s)\} &= \frac{1}{2L}\int_{-L}^{L} \exp[2\pi\mathrm{i}k\sin(\pi y/L)]\mathrm{d}y \\ &= \frac{1}{2\pi}\int_{0}^{2\pi} \exp(-2\pi\mathrm{i}k\sin\theta)\mathrm{d}\theta = J_0(2\pi k).\end{aligned} \tag{31}$$

The corresponding inverse Fourier transform of Eq. (31) is

$$F_\Delta(s) = \frac{1/\pi}{\cos(\arcsin s)} = \frac{1/\pi}{\sqrt{1 - s^2}} \tag{32}$$

(see also Fig. 3). In spite of the strong similarity between the Fourier transform of $F_\Delta(s)$ for the sinusoidal field with that of the shear field (see Fig. 3, middle), the corresponding displacement distributions are quite different: the distribution for the sinusoidal field has *two* peaks. This means that the displacement-correlation peak will have two maxima (provided that the local variations of the displacement field are larger than the equivalent width of the particle images; see discussion below). This is an example of the so-called *peak splitting*, which occurs often in regions with very strong local fluctuations of the displacement. This means that for a finite number of particle images the interrogation analysis will only detect one of the two peaks; in this case the measured displacement can *not* be considered as a local mean value of the displacement field.

4 The displacement-correlation peak for non-uniform displacements

The analysis in the preceding section did not include the effects due to the finite window size and the finite dimensions of the particle images. Our point of departure is the exact expression in Eq. (8). For ideal tracer particles the two-point correlation of the tracer-pattern fluctuations for a *non-uniform* displacement field is given by, cf. Eq. (9)

$$\left\langle g_1'(\boldsymbol{x}')g_2'(\boldsymbol{x}'')|\boldsymbol{u}\right\rangle = C\delta[\boldsymbol{x}'' - \boldsymbol{x}' - \Delta\boldsymbol{x}(\boldsymbol{x}')]. \tag{33}$$

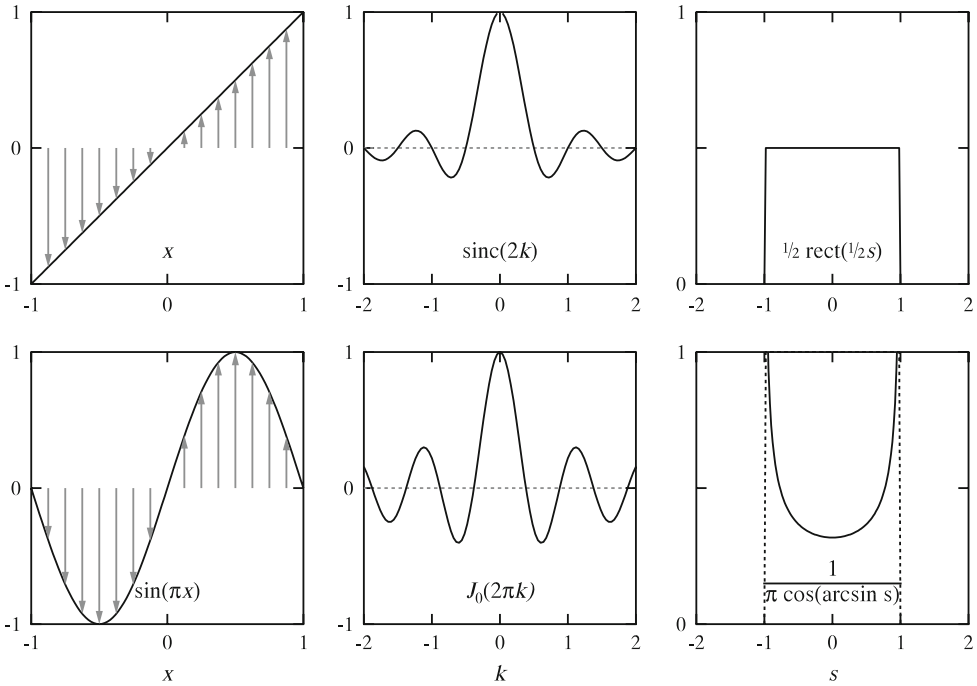

Fig. 3 The displacement field (*left*), and the corresponding distribution Fourier transform (*middle*) and displacement distribution (*right*), for a simple shear (*top row*) and sinusoidal displacement field (*bottom row*)

In the case of a uniform displacement field, $\langle g'_1(\boldsymbol{x}')g'_2(\boldsymbol{x}'')|\boldsymbol{u}\rangle$ is a function of $\boldsymbol{s} = \boldsymbol{x}'' - \boldsymbol{x}'$ only, which leads to a rather simple expression that was derived in Sect. 2. However, for a non-unform displacement field Eq. (33) is a function of $\boldsymbol{x}'$, which makes it difficult to carry out a straightforward evaluation of Eq. (8). The expression in Eq. (8) can be solved numerically, but this is a rather cumbersome procedure for a generalized analysis of spatial gradients. Instead, it is possible to reduce Eq. (8) to that of a much simpler approximate equation, by making some general assumptions. This procedure is described in this section.

4.1 Approximate expression

To simplify the expression in Eq. (8), it is assumed that the displacement field is uniform, except in the direction of the x-coordinate, i.e.,

$$\Delta\boldsymbol{x}(\boldsymbol{x}) = (\Delta x(\boldsymbol{x}), \Delta y, \Delta z)^T. \tag{34}$$

It is assumed that the displacement field is a function of x and y only, so that the double integral over z' and z'' can be replaced by

$$\iint I_{01}(z')I_{02}(z'')\delta(z'' - z' - \Delta z)\mathrm{d}z'\,\mathrm{d}z'' = I_{z1}I_{z2}\Delta z_0 F_{\mathrm{O}}(\Delta z) \tag{35}$$

In order to preserve the skewing effect of the in-plane loss-of-pairs on the displacement-correlation peak, a term containing $F_I(\boldsymbol{s})$ is split from the integrand:

$$\begin{aligned}\int W_1(\boldsymbol{X})W_2(\boldsymbol{X}+\boldsymbol{s})\cdots\mathrm{d}\boldsymbol{X} &\Rightarrow F_I(\boldsymbol{s})D_I^2 \\ \times \int \frac{W_1(\boldsymbol{X})W_2(\boldsymbol{X}+\boldsymbol{s})}{F_I(\boldsymbol{s})D_{\mathrm{I}}^2}\cdots\mathrm{d}\boldsymbol{X}&.\end{aligned} \tag{36}$$

In addition, the particle-image self-correlation is accounted for by a convolution of the integrand with $F_\tau(\boldsymbol{s})$

$$\begin{aligned}&\iiint \tau_0(\boldsymbol{X}-\boldsymbol{X}')\tau_0(\boldsymbol{X}+\boldsymbol{s}-\boldsymbol{X}'')\cdots\mathrm{d}\boldsymbol{X}\,\mathrm{d}\boldsymbol{X}'\,\mathrm{d}\boldsymbol{X}'' \\ &\quad\Rightarrow \tau_{00}^2\int F_\tau(\boldsymbol{s}-\boldsymbol{s}')\left\{\iiint \delta(\boldsymbol{X}-\boldsymbol{X}')\delta(\boldsymbol{X}+\boldsymbol{s}'-\boldsymbol{X}'')\cdots\right. \\ &\left.\cdots\mathrm{d}\boldsymbol{X}\,\mathrm{d}\boldsymbol{X}'\,\mathrm{d}\boldsymbol{X}''\right\}\mathrm{d}\boldsymbol{s}'.\end{aligned} \tag{37}$$

The substitution of Eqs. (35)–(37) in Eq. (8) yields

$$\begin{aligned}\langle R_D(\boldsymbol{s})|\boldsymbol{u}\rangle \cong I_{z1}I_{z2}\tau_{00}^2 N_{\mathrm{I}}F_{\mathrm{O}}(\Delta z)F_{\mathrm{I}}(\boldsymbol{s})&\int F_\tau(\boldsymbol{s}-\boldsymbol{s}') \\ \times\iiint \frac{W_1(\boldsymbol{X})W_2(\boldsymbol{X}+\boldsymbol{s}')}{F_{\mathrm{I}}(\boldsymbol{s}')D_{\mathrm{I}}^2}&\\ \times\delta(\boldsymbol{X}-\boldsymbol{X}')\delta(\boldsymbol{X}+\boldsymbol{s}'-\boldsymbol{X}'')&\\ \times\delta[\boldsymbol{X}''-\boldsymbol{X}'-\Delta\boldsymbol{X}(\boldsymbol{X}')]\mathrm{d}\boldsymbol{X}\,\mathrm{d}\boldsymbol{X}'\,\mathrm{d}\boldsymbol{X}''\,\mathrm{d}\boldsymbol{s}'&\end{aligned} \tag{38}$$

with: $\Delta\boldsymbol{X} = M\Delta\boldsymbol{x}$. This expression is then further reduced by the integration of the two δ-functions that replace the τ_0-functions, i.e.

$$\begin{aligned}\langle R_D(\boldsymbol{s})|\boldsymbol{u}\rangle = I_{z1}I_{z2}\tau_{00}^2 N_{\mathrm{I}}F_{\mathrm{O}}(\Delta z)F_{\mathrm{I}}(\boldsymbol{s})&\int F_\tau(\boldsymbol{s}-\boldsymbol{s}') \\ \times\int \frac{W_1(\boldsymbol{X}')W_2(\boldsymbol{X}'+\boldsymbol{s}')}{F_{\mathrm{I}}(\boldsymbol{s}')D_{\mathrm{I}}^2}&\delta[\boldsymbol{s}'-\Delta\boldsymbol{X}(\boldsymbol{X}')]\mathrm{d}\boldsymbol{X}'\,\mathrm{d}\boldsymbol{s}'.\end{aligned} \tag{39}$$

Given that the variations of the displacement field are small, i.e.,

$$\boldsymbol{s}' \approx \boldsymbol{s}_D = \Delta \boldsymbol{X}(\boldsymbol{X}_0) \tag{40}$$

with $|a| = M|\Delta u|\Delta t \ll D_\mathrm{I}$, $F_\mathrm{I}(\boldsymbol{s}')$ is replaced by $F_\mathrm{I}(\boldsymbol{s}_D)$, so that $F_\mathrm{I}(\boldsymbol{s}_D)D_I^2$ represents the normalization constant for the displacement distribution function. Hence, the approximation for Eq. (8) reads

$$\langle R_D(\boldsymbol{s})|\boldsymbol{u}\rangle \cong I_{z1}I_{z2}\tau_{00}^2 N_\mathrm{I} F_\mathrm{O}(\Delta z) F_\mathrm{I}(\boldsymbol{s}) \times \int F_\tau(\boldsymbol{s}-\boldsymbol{s}')F_\Delta(\boldsymbol{s}')\mathrm{d}\boldsymbol{s}', \tag{41}$$

with

$$F_\Delta(\boldsymbol{s}') = \frac{1}{F_\mathrm{I}(\boldsymbol{s}_D)D_\mathrm{I}^2}\int W_1(\boldsymbol{X}')W_2(\boldsymbol{X}'+\boldsymbol{s}') \times \delta[\boldsymbol{s}' - \Delta\boldsymbol{X}(\boldsymbol{X}')]\mathrm{d}\boldsymbol{X}'. \tag{42}$$

Note that the integral in Eq. (41) represents a convolution of $F_\tau(\boldsymbol{s})$ and $F_\Delta(\boldsymbol{s})$; this justifies the expression given in Eq. (22).

Evidently, the result in Eqs. (41–42) needs to be validated against the numerical solutions of the exact expression in Eq. (8). This is done in the next section.

4.2 Simple flows

In this section the effect of spatial gradients in the displacement field on the location, height and shape of the displacement-correlation peak is investigated for the case of simple, one-dimensional displacement fields, such as simple shear and uniaxial strain. To reduce the complexity of the analysis, only uniform interrogation windows are considered. Analytical expressions for the peak centroid and the peak width are found by means of the approximate expression Eq. (41) that was derived in the preceding section. These are compared against numerical solutions of the exact expression Eq. (8).

4.2.1 Simple shear

Consider a uniform displacement ΔX_0 plus a simple shear motion

$$\Delta X(Y) = \Delta X_0 + \frac{a}{D_\mathrm{I}}\cdot(Y - Y_0). \tag{43}$$

The displacement field is a function of Y only, so that $F_\Delta(\boldsymbol{s})$, defined in Eq. (42), is given by

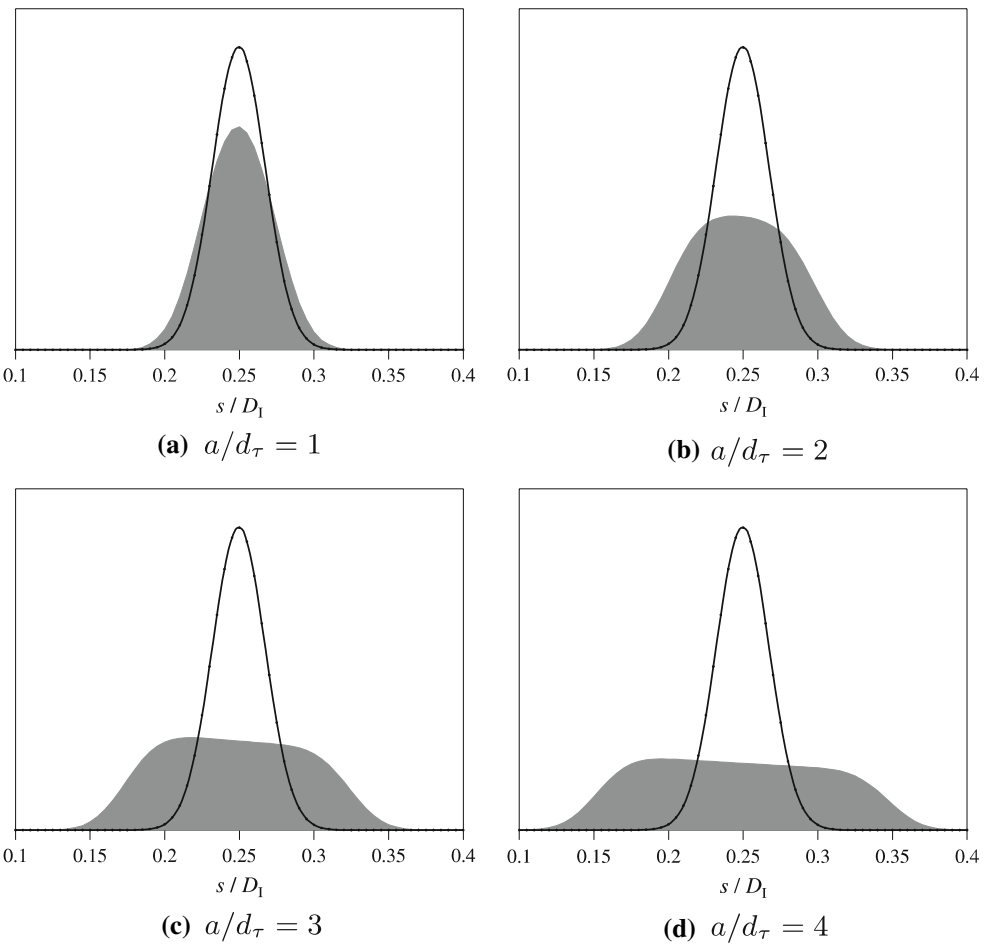

Fig. 4 The displacement-correlation peak for the case of simple shear for different values of the gradient parameter a (=$M\Delta u\Delta t$) relative to the particle-image diameter d_τ, with a mean displacement of $\Delta X_0 = 0.25D_\mathrm{I}$ and a particle-image diameter $d_\tau = 0.05D_\mathrm{I}$. The curve represents the displacement-correlation peak for a uniform displacement that is equal to the mean displacement of the shear motion

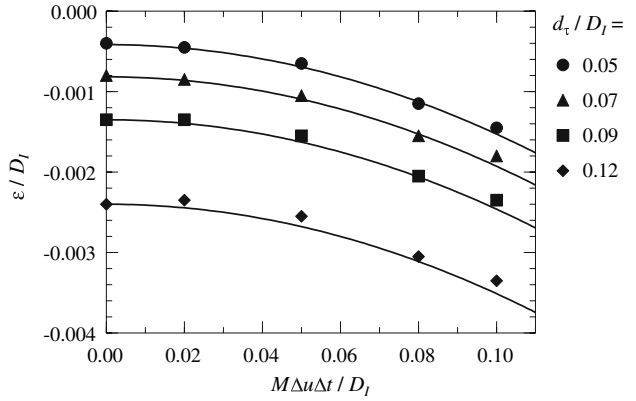

Fig. 5 The displacement bias ε ($=\mu_D - s_D$) relative to D_I as a function of the local variation of the displacement $M\Delta u\Delta t$ for a uniform simple shear plus a uniform translation of $\Delta X_0 = 0.25D_\mathrm{I}$, for different values of d_τ/D_I

$$F_\Delta(s,t) = \delta(t) \cdot \frac{1}{D_\mathrm{I}} \int_W \delta[s - M\Delta x(Y)]\mathrm{d}Y, \tag{44}$$

with $\boldsymbol{s} = (s,t)^T$. This integral was solved in Sect. 3 for a uniform simple shear and a uniform interrogation window. Hence, the corresponding displacement distribution $F_\Delta(s,t)$ is uniform in s:

$$F_\Delta(s,t) = \delta(t) \cdot \frac{1}{|a|} \cdot \begin{cases} 1 & |s| \le \frac{1}{2}|a|, \\ 0 & \text{elsewhere.} \end{cases} \tag{45}$$

The substitution of Eq. (45) in Eq. (41) yields the displacement-correlation peak that is shown in Fig. 4 for different values of the gradient parameter a. In the Gaussian approximation for $F_\tau(\boldsymbol{s})$ and $F_\Delta(\boldsymbol{s})$, the width d_D of $F_\tau * F_\Delta(\boldsymbol{s})$ is given by

$$d_D \cong \sqrt{2d_\tau^2 + \frac{4}{3}(M|\Delta u|\Delta t)^2}. \tag{46}$$

Hence, the local shear motion increases the width of the displacement-correlation peak. This increases the displacement bias error of the peak centroid in comparison to the uniform displacement result Eq. (21)

$$\frac{\mu_D - s_D}{D_\mathrm{I}} = -\frac{1}{F_\mathrm{I}(s_D)}\frac{d_\tau^2}{8D_\mathrm{I}^2} - \frac{1}{F_\mathrm{I}(s_D)}\frac{(M|\Delta u|\Delta t)^2}{12D_\mathrm{I}^2}. \tag{47}$$

In Fig. 5 the displacement bias error is plotted as a function of the gradient parameter for different particle-image diameters. The solid lines represent Eq. (47), whereas the symbols are numerical solutions of the exact equation in Eq. (8). Note that the *increase* of the bias magnitude due to the shear is equal for all values of d_τ. This is reflected in Fig. 6, in which the width of the displacement-correlation peak relative to its width for uniform displacements (i.e., $\sqrt{2}d_\tau$) is plotted as a function of the gradient relative to the particle-image diameter. The solid line represents Eq. (46),

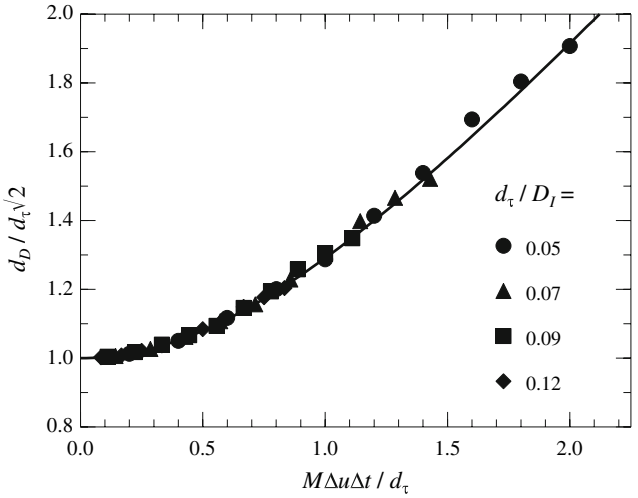

Fig. 6 The width d_D of $\langle R_D|\boldsymbol{u}\rangle$ relative to the particle-image diameter d_τ as a function of the local variation of the displacement $M\Delta u\Delta t$ relative to d_τ

whereas the symbols represent numerical solutions of Eq. (8). This graph indicates that PIV images with large d_τ are less sensitive to variations in the displacement than those images with small d_τ. So, according to Eq. (18) the displacement bias error is determined by the width d_D of the displacement-correlation peak, given by Eq. (47). This is shown in Fig. 7, in which the displacement bias error is plotted as a function of d_D.

4.2.2 *Uniaxial strain*

Consider the displacement field for uniaxial strain

$$\Delta X(X) = \Delta X_0 + \frac{a}{D_\mathrm{I}} \cdot (X - X_0), \tag{48}$$

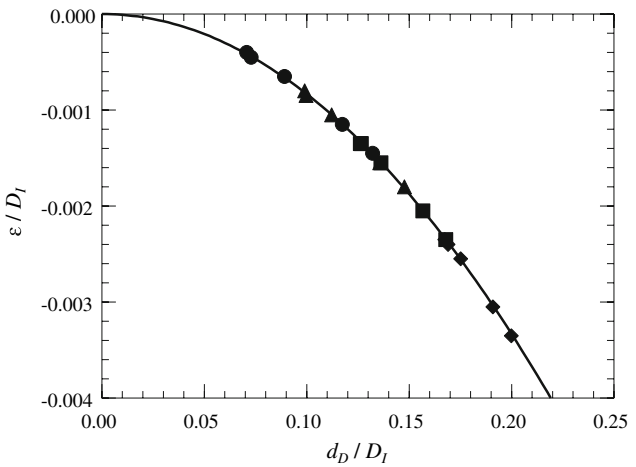

Fig. 7 The displacement bias ε relative to D_I as a function of the width d_D of $\langle R_D|\boldsymbol{u}\rangle$ relative to D_I. The symbols correspond to the data in Fig. 6, and the solid line represents Eq. (47)

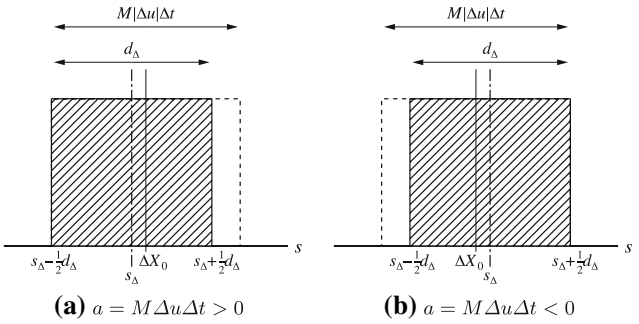

Fig. 8 The displacement distribution for uniaxial strain. For positive strain (**a**) the distribution is truncated at the largest displacements, whereas for negative strain (**b**) the distribution is truncated at the smallest displacements

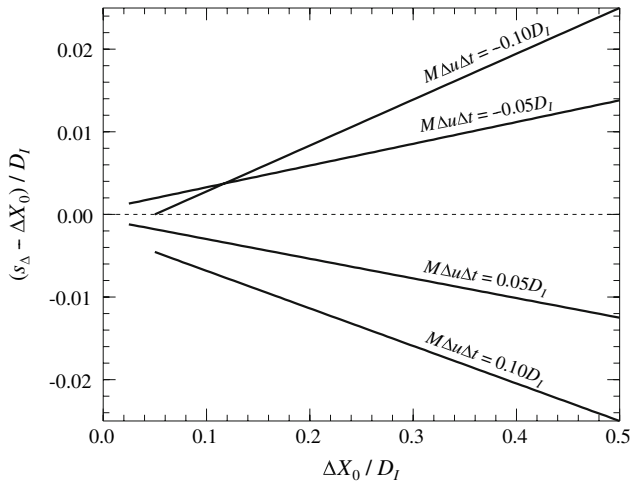

Fig. 9 The first moment of the displacement distribution for a uniaxial strain as a function of the local mean displacement ΔX_0, for different values of the gradient parameter $a = M\Delta u\Delta t$

with $\frac{1}{2}|a| \leq \Delta X_0$, so that $\Delta X \geq 0$ for all positions inside the interrogation window. Substitution of Eq. (48) in Eq. (42) yields

$$F_\Delta(s,t) = \delta(t) \cdot \frac{1}{F_I(s_D,0)D_I} \times \int W_1(X)W_2(X+s)\,\delta[s-\Delta X(X)]\mathrm{d}X \tag{49}$$

(Note that W_1 and W_2 now represent one-dimensional functions.) The integrand only makes a contribution to the total integral when $s = \Delta X(X)$ on the interval where $W_1(X)W_2(X + s) \neq 0$. This implies that the finite dimensions of the interrogation windows limit the range of displacements that can be measured.

As for the case of a simple shear, the displacement distribution of the tracer particles within W_1 is uniform with a mean displacement ΔX_0 and a width $M|\Delta u|\Delta t$. However, for $\Delta x > 0$ the integral in Eq. (49) is non-zero only for

$$\Delta X(X_I - \frac{1}{2}D_I) < s < \Delta X(X_I + \frac{1}{2}D_I - s). \tag{50}$$

Substitution of Eq. (48) yields that $F_\Delta(s) \neq 0$ for $|s - s_\Delta| < \frac{1}{2}d_\Delta$, with (see also Fig. 8)

$$d_\Delta = \frac{|a|/D_I}{1 + a/D_I}\left[1 - \frac{\Delta X_0}{D_I} + \frac{1}{2}\frac{a}{D_I}\right]D_I \tag{51}$$

and:

$$s_\Delta = \Delta X_0 - \frac{1}{2}\frac{a}{D_I}\left[1 - \frac{d_\Delta}{|a|}\right]D_I. \tag{52}$$

Hence, for the case of a *positive* uniaxial strain ($a = M\Delta u\,\Delta t > 0$), i.e., a spatially accelerating fluid, Eq. (49) implies that the local displacement-distribution is truncated at the side of the largest displacements. Consequently, the mean of the *observed* local displacement-distribution is then biased toward a smaller displacement in comparison with the actual mean of the local displacement distribution. On the other hand, for a *negative* uniaxial strain ($a = M\Delta u\,\Delta t < 0$), i.e., a spatially decelerating fluid, the distribution is truncated at the side of *smallest* displacements, so that the mean measured displacement is *larger* than the local mean displacement. This bias adds to the displacement bias error that is the result of the skew of the displacement-correlation peak due to F_I (Fig. 9).

So, for an accelerating fluid ($a > 0$) the measured displacement is smaller than the true local mean displacement, whereas for a decelerating fluid ($a < 0$) the measured displacement is larger. It is as if the tracer particles have some inertia, even if the tracer particles themselves are *ideal*.

The effect of the uniaxial strain on the centroid of the displacement-correlation peak is found by the substitution of $F_\Delta(s)$ in Eq. (22). In Fig. 10 are shown the displacement-correlation peaks for uniaxial strain with different values of a. Note that the displacement-correlation peak for uniaxial strain has a larger bias than for simple shear (for the same value of a), which is the result of the truncation of the displacement distribution for large displacements.

To estimate the displacement bias error, it is assumed that the width d_D of the displacement-correlation peak for a uniaxial normal stress is given by (Gaussian approximation):

$$d_D \cong \sqrt{2d_\tau^2 + \frac{1}{12}\left[\frac{a/D_I}{1 + a/D_I}\left(1 - \frac{\Delta X_0}{D_I} + \frac{1}{2}\frac{a}{D_I}\right)\right]^2}. \tag{53}$$

In Fig. 12 the approximate result in Eq. (53) is compared against the numerical solutions of the equation in Eq. (22).

The total displacement bias error is now given by the displacement bias error for the truncated displacement distribution *plus* the bias error due to the increase of the width of the displacement-correlation peak, i.e.:

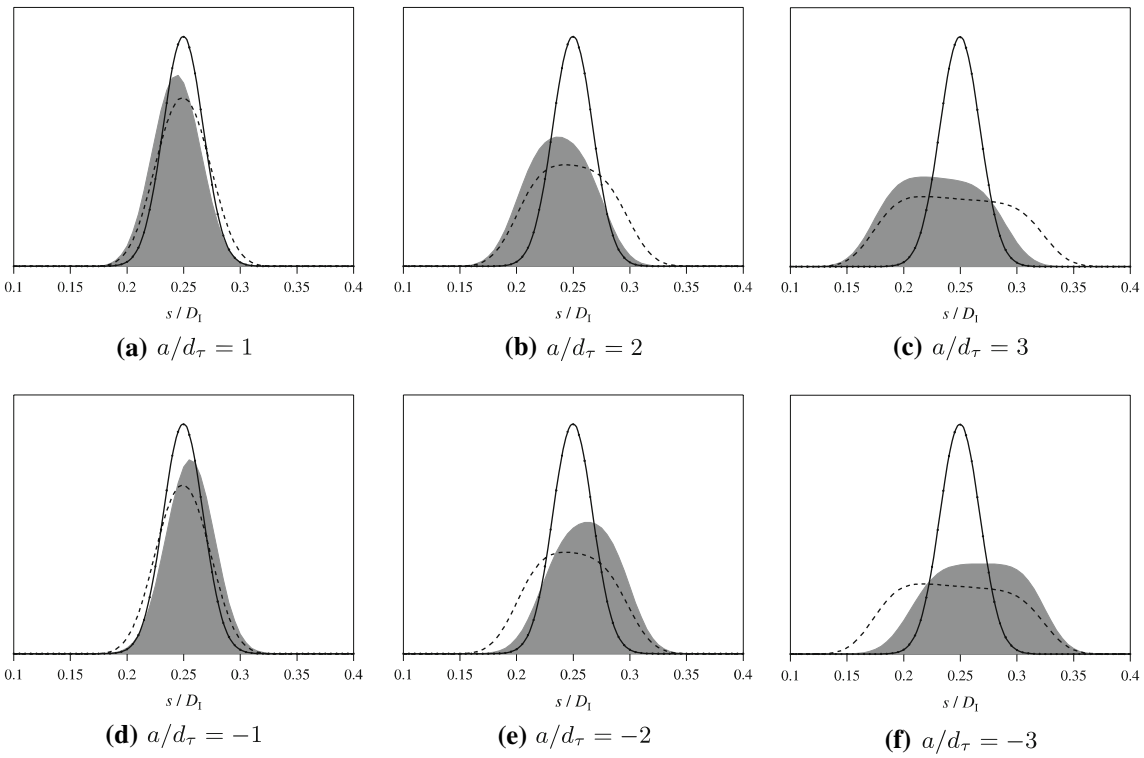

Fig. 10 As Fig. 4, but now for uniaxial strain, i.e., spatially accelerating ($a > 0$) or decelerating ($a < 0$) fluid. The dashed curves correspond to the displacement-correlation peaks for a simple shear in Fig. 4

$$\frac{s_D - \Delta X_0}{D_\mathrm{I}} = -\frac{1}{F_I(s_D)}\frac{d_D^2}{16D_I^2} - \frac{1}{2}\frac{a/D_\mathrm{I}}{1 + a/D_\mathrm{I}}\left[\frac{\Delta X_0}{D_\mathrm{I}} + \frac{1}{2}\frac{a}{D_\mathrm{I}}\right]. \tag{54}$$

The total displacement bias error for uniaxial strain is plotted in Fig. 11. It is noted that the use of offset interrogation windows, which implies $\Delta X_0 = 0$, only compensates for part of the bias and increase in peak width (Fig. 12).

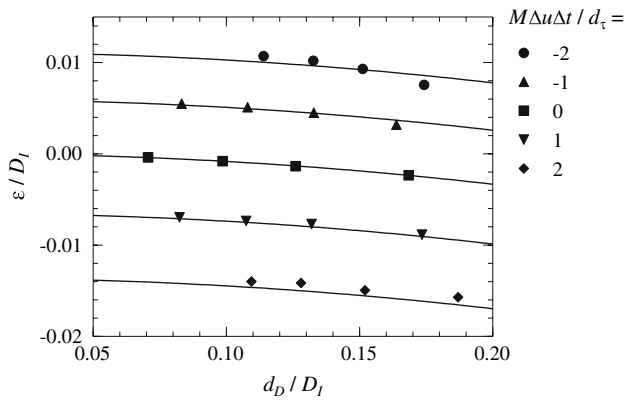

Fig. 11 The displacement bias error for uniaxial strain as a function of the correlation peak width d_D, for different values of $M\,\Delta u\,\Delta t$. The mean displacement ΔX_0 is $0.25D_\mathrm{I}$. The *solid lines* correspond to Eq. (54); the symbols are obtained from numerical solutions of Eq. (8)

5 Discussion and conclusion

The previous sections describe the effect of local gradients at the scale of the interrogation domain on the shape of the displacement-correlation peak. This is a generalization of the existing theoretical expression for the displacement-correlation peak. An approximate expression is derived,

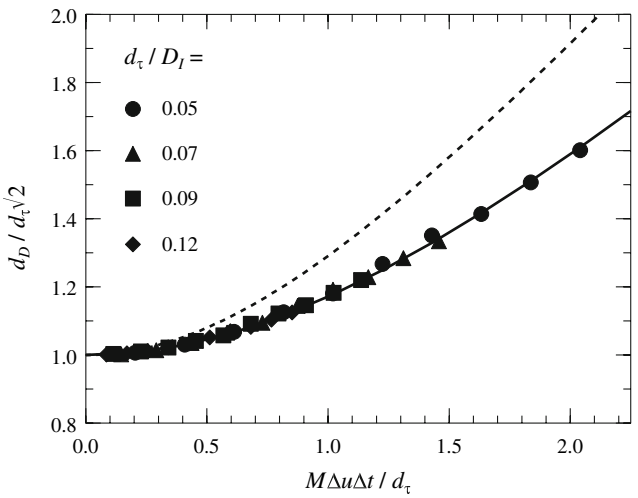

Fig. 12 As Fig. 6, but now for a uniaxial strain (with $\Delta X_0 = 0.25D_\mathrm{I}$). The *solid curve* represents Eq. (54); the *dashed curve* corresponds to the *solid curve* in Fig. 6

which accurately predicts the bias error and peak width for simple flows. It is confirmed that the broadening and splitting of the displacement-correlation peak due to local variations of the displacement does not occur as long as the variation a of the displacements over the interrogation volume does not exceed the particle image diameter d_τ, as stated in Eq. (1).

The procedure to determine the displacement-correlation peak for non-uniform displacement fields would be as follows:

1. determine the local distribution function $F_\Delta(\boldsymbol{s})$ of the displacement field;
2. convolve $F_\Delta(\boldsymbol{s})$ with the particle-image self-correlation $F_\tau(\boldsymbol{s})$;
3. multiply the result with the in-plane loss-of-pairs $F_I(\boldsymbol{s})$ and out-of-plane loss-of-pairs $F_O(\Delta z)$.

In most situations with small values of a the local displacement field is well approximated by a uniform displacement *plus* a shear and/or uniaxial strain. Specific results for these fluid motions are obtained in Sects. 4.2.1 and 4.2.2.

The principal effect of sub-interrogation gradients is a reduction of the peak amplitude, a bias error in the estimated displacement, and a proportional broadening of the correlation peak, where the total volume of the correlation peak is conserved. The analysis predicts the bias error and correlation peak width, which can be related to peak detectability (peak height) and random error (peak width). For a simple shear the width d_D of the correlation peak is given by Eq. (46). The conservation of total volume then implies that the correlation peak amplitude is given by

$$R_D(\boldsymbol{s}_D) \sim N_I F_I F_O F_\Delta \quad \text{with,} \quad F_\Delta \cong \exp\left(-\frac{2}{3}a^2/d_\tau^2\right). \tag{55}$$

This expression predicts mean peak amplitudes of: 1.00, 0.85, 0.51 and 0.22, for: a/d_τ = 0.0, 0.5, 1.0 and 1.5, respectively; these values correspond well with the (instantaneous) peak amplitudes shown in Fig. 1 (see also Hain and Kähler 2007). The *one-quarter rules* for the in-plane and out-of-plane displacement imply a maximum loss-of-correlation that reduces the correlation peak height to 75% of the maximum amplitude. A similar drop in amplitude corresponds to $|a|/\ d_\tau < 0.66$, i.e., a *two-third rule* for the displacement variation.

The random error $\sigma_{\Delta X}$ is proportional to the width d_D of the displacement-correlation peak, and for a simple shear it is approximately given by[6]

$$\sigma_{\Delta X} \cong c\ d_D/\sqrt{2} \cong c\ d_\tau\sqrt{1+\frac{2}{3}a^2/d_\tau^2}, \tag{56}$$

with c = 0.05-7 (Westerweel 2000b).

In the case of a uniaxial strain, i.e., a spatially accelerating or decelerating fluid, the centroid of the displacement-correlation peak yields an additional bias that can be interpreted as an artificial 'inertia' of the particles. This even occurs when the particles can be considered as ideal tracers, and is the result of the finite dimensions of the interrogation domain.

Also, the analysis shows that a simple sinusoidal fluid motion with a wavelength equal or less than the dimension of the interrogation domain leads to the appearance of two correlation peaks (see Fig. 3) when the displacement amplitude becomes larger than d_τ. This is an example of the so-called *peak splitting*. In a practical situation, i.e., with a finite number of particle images, it is likely that the interrogation analysis just finds only one of the two peaks (ignoring the other peak as a possible random-correlation peak). Then the measured displacement would correspond to the local *minimum* or *maximum* displacement.[7] This means that the measured displacement for the case of a sinusoidal displacement field is *not* proportional to the locally averaged displacement; this invalidates the commonly accepted assumption that the measured displacement is equal to the locally averaged displacement (Willert and Gharib 1991; Olsen and Adrian 2001; Hart 2000; Nogueira et al. 1999).

An application where the local gradients can become dominant is micro-PIV, in particular for measurements where the interrogation domain extends over a substantial part along the observation direction. For pressure-driven Stokes flow in a channel geometry the velocity profile along the optical axis has a parabolic shape. This shape is approximated by the sinusoidal distribution in Fig. 3 for: $0 \le x \le 1$; hence, $F_\Delta(s)$ is approximately given by Eq. (32) for $s \ge 0$. This particular shape of the displacement-correlation peak is reported by Wereley and Whitacre (2006). In this particular situation the PIV measurement yields the *maximum* velocity in the measurement domain, rather than the *mean* displacement.

In order to absorb larger local variations of the displacement, one could increase the particle-image diameter d_τ. In the case of diffraction-limited particle images, $d_\tau \approx d_s$, with $d_s = 2.44(M+1)f^\#\lambda$, where $f^\#$ is the aperture number of the lens and λ the light wavelength. So, d_τ can be increased by increasing $f^\#$, i.e., by reducing the lens aperture. Unfortunately, this also reduces the collected amount of light scattered by the tracer particles, and—in

[6] Provided that the particle image diameter is at least two pixel units in a digital PIV image.

[7] As the result of the bias toward $\boldsymbol{s} = \boldsymbol{0}$, it is more likely that the peak closest to the origin of the correlation domain is detected.

the case of micro-PIV—implies an unfavorable increase of the correlation depth (Olsen and Adrian 2000b). An increase of d_τ also implies a proportional increase of the random error, given in Eq. (56), and a general deterioration of the overall performance of the PIV system (Adrian 1997). One could possibly determine an optimum between increasing d_τ to improve peak detectability, while accepting a (small) increase in the random error. The expressions given in this paper can be used as a guideline.

References

Adrian RJ (1984) Scattering particle characteristics and their effect on pulsed laser measurements of fluid flow: speckle velocimetry vs. particle image velocimetry. Appl Opt 23:1690–1691

Adrian RJ (1988) Statistical properties of particle image velocimetry measurements in turbulent flow. In: Adrian RJ et al (eds) Laser anemometry in fluid mechanics – III. Ladoan-Inst Super Tec, Lisbon, pp 115–129

Adrian RJ (1997) Dynamic ranges of velocity and spatial resolution of particle image velocimetry. Meas Sci Technol 8:1393–1398

Fincham A, Delerce G (2000) Advanced optimization of correlation imaging velocimetry algorithms. Exp Fluids 29:S13–S22

Hain R, Kähler CJ (2007) Fundamentals of multiframe particle image velocimetry (PIV). Exp Fluids 42:575–587

Hart DP (2000) PIV error correction. Exp Fluids 29:13–22

Hohreiter V, Wereley ST, Olsen MG, Chung JN (2002) Cross-correlation analysis for temperature measurement. Meas Sci Technol 13:1072–1078

Huang HT, Fiedler HE, Wang JJ (1993) Limitation and improvement of PIV. Part i: limitation of conventional techniques due to deformation of particle image patterns. Exp Fluids 15:168–174

Keane RD, Adrian RJ (1990) Optimization of particle image velocimeters. Part I: double pulsed systems. Meas Sci Technol 1:1202–1215

Keane RD, Adrian RJ (1992) Theory of cross-correlation analysis of PIV images. Appl Sci Res 49:191–215

Nogueira J, Lecuona A, Rodriguez PA (1999) Local field correction PIV: on the increase of accuracy of digital PIV systems. Exp Fluids 27:107–116

Olsen MG, Adrian RJ (2000a) Brownian motion and correlation in particle image velocimetry. Opt Laser Technol 32:621–627

Olsen MG, Adrian RJ (2000b) Out-of-focus effects on particle image visibility and correlation in microscopic particle image velocimetry. Exp Fluids 29:S166–S174

Olsen MG, Adrian RJ (2001) Measurement volume defined by peak-finding algorithms in cross-correlation particle image velocimetry. Meas Sci Technol 12:N14–N16

Prasad AK (2000) Stereoscopic particle image velocimetry. Exp Fluids 29:103–116

Scarano F (2002) Iterative image deformation methods in PIV. Meas Sci Technol 13:R1–R19

Tokumaru PT, Dimotakis PE (1995) Image correlation velocimetry. Exp Fluids 19:1–15

Wereley ST, Whitacre I (2006) Particle dynamics in a dielectrophoretic microdevice. In: Ferrari M, Bashir R, Wereley S (eds) BioMEMS and biomedical nanotechnology. Volume IV: biomolecular sensing, processing and analysis, chapter 13. Springer, Heidelberg, pp 259–276

Westerweel J (1993) Digital particle image velocimetry—theory and application. PhD thesis, Delft University of Technology

Westerweel J (1997) Fundamentals of digital particle image velocimetry. Meas Sci Technol 8:1379–1392

Westerweel J (2000a) Effect of sensor geometry on the performance of PIV interrogation. In: Adrian RJ, et al (eds) Laser techniques applied to fluid mechanics. Springer, Berlin, pp 37–55

Westerweel J (2000b) Theoretical analysis of the measurement precision in particle image velocimetry. Exp Fluids 29:S3–12

Westerweel J (2004) Principles of PIV technique III. Spatial correlation analysis. In: Application of particle image velocimetry—theory and practice. DLR, Göttingen

Westerweel J, Dabiri D, Gharib M (1997) The effect of a discrete window offset on the accuracy of cross-correlation analysis of digital PIV recordings. Exp Fluids 23:20–28

Willert CE, Gharib M (1991) Digital particle image velocimetry. Exp Fluids 10:181–193